The Machine Learning Enabled Thermosphere Advanced by the High Accuracy Satellite Drag Model (META-HASDM)

Kent Tobiska, Bruce Bowman
Space Environment Technologies

Marcin D. Pilinski
University of Colorado at Boulder / Laboratory for Atmospheric and Space Physics

Piyush Mehta and Richard Licata
West Virginia University

ABSTRACT SUMMARY

The number of Low Earth Orbit (LEO) objects will TRIPLE in the next 2 years and collisional hazards will increase. The Machine learning Enabled Thermosphere Advanced by HASDM (META-HASDM) system is a collaborative project between Space Environment Technologies and West Virginia University. It will significantly reduce uncertainty in thermospheric density specification and will improve conjunction assessment as well as operational global space traffic management. META-HASDM, in particular, will aid with space weather forecasting technologies and techniques by providing: i) information for scientific and operational use via new machine learning (ML) algorithms; absolute atmosphere density at HASDM's current 2–10% uncertainty algorithmically; ii) predicted values for outside HASDM's historic time period; iii) improved LEO ballistic coefficients above 500 km; iv) dynamic uncertainties for HASDM, JB2008, and forecast drivers; and v) improved forecasts for solar and geomagnetic indices. In addition, META-HASDM already provides a new space weather benchmark with the two solar cycle SET HASDM density database that has been released publicly at https://spacewx.com/hasdm/ and accuracy, time resolution, and global scale, where no comparable dataset currently exists. In this paper, we report on the progress of META-HASDM.

1. INTRODUCTION

The number of LEO objects will TRIPLE in the next 2 years and this stuns us. Behind this is the drive for a high-speed internet, the life blood of our global economy and national defense. Commercial efforts, such as SpaceX's Starlink constellation, but not limited to them, are hugely expanding global internet capacity in the next two years. At the time of this paper (September 2021), SpaceX's Starlink has 1600 satellites in Low Earth Orbit (LEO) at 550 km with a goal of orbiting up to 42,000 total satellites in that region. In January 2019 there were already 34,000 objects in Earth orbit larger than 10 cm (a grapefruit) of which 2/3 of that population (23,000) was in LEO.

The Starlink systems, along with all of NASA's active satellites, will be joined by the entire satellite fleet that will see active management within of the emerging Space Traffic Management (STM) paradigm of the Department of Commerce (DoC). All these government systems, including NASA's Conjunction Assessment Risk Analysis (CARA) program supporting conjunction assessment (CA), depend upon the functioning of one thing – the U.S. Space Force (USSF) Space Command's High Accuracy Satellite Drag Model (HASDM). HASDM [1] is a data assimilative system combined with an empirical forecast model. It provides the most accurate atmospheric density and object locations to its users. However, it is only as good as its underlying uncertainty. Furthermore, the advanced utility of the HASDM model has not been available to most users outside the DoD and NASA CARA.

The primary objective of this work is to provide a parametrized model of the thermosphere that is based on a recent public release of 20-years of HASDM data. We use machine learning (ML) to capture the principal modes in the available HASDM database and present them as an empirical model (META-HASDM) that can be used by a wider community. Another goal is to provide the percent error of atmospheric density, which has been identified as the key component needed to account for mismodeling of the current epoch and forecast atmosphere density [2]. Hejduk and Snow show in that work that if the atmosphere density uncertainty is known, then the square of that uncertainty can

be directly added to the normalized ballistic coefficient variance. The result is a probability of collision between two satellites that can be more accurately predicted, allowing operators to reduce false positive and false negative collision predictions. These operators are the end users like NASA CARA, NASA ISS, SpaceX Starlink, other agencies' high value satellites, and commercial LEO satellites that will be working with DoC STM. Finally, HASDM neutral densities, and therefore the META-HASDM outputs resulting from this work, are calibrated by satellite drag observations via a specific drag coefficient (C_D) coefficient model. This C_D model is verified by comparing the HASDM public database with drag observations across a wide range of altitudes. The results are published here so that users of META-HASDM and the public HASDM database can compute unbiased drag values for any LEO object.

In this paper we describe the META-HASDM machine learning methodology. Next, the principal components of the HASDM database are analyzed. Error characteristics of the META-HASDM density model are then presented. Finally, we present recommendations for computing unbiased drag estimates using the META-HASDM model by adopting specific, altitude dependent, drag coefficient models.

2. METHODOLOGY

Access to the HASDM density database

Under authority from USSF, Space Environment Technologies (SET) has extracted two solar cycles of temperature-corrected coefficients to create the SET HASDM density database. This is the first-time there has been an extraction of this operational database for scientific use [3]; there is no comparable dataset in existence and the densities in this database are those used by groups such as NASA CARA for the last two solar cycles. The information content in the database inherently includes all the geomagnetic storm and sub-storm, extended solar flare, nitric oxide (NO) and carbon dioxide (CO_2) thermospheric cooling perturbations. Because of its accuracy, time resolution, global scale, and information content, the SET HASDM database densities are now used as a new space weather benchmark for atmospheric expansion. This database will help refine the Phase 1 Benchmark that was released by the National Science and Technology Council [4] for upper atmospheric expansion.

The global density SQL database from January 1, 2000 to December 31, 2019 has 3-h time resolution, 25-km altitude steps and a 175–825 km altitude range on a 10° × 15° latitude/longitude grid. This database is publicly available for scientific research use and is located at the URL https://spacewx.com/hasdm/. Figure 1 shows an example of the output of the SET HASDM density database at 400 km for the October 30, 2003 Halloween storm period at 00:00 UT. It is this database that we will use to assess uncertainties of the JB2008 model forecasts. The uncertainties in the HASDM database are discussed in the ML section.

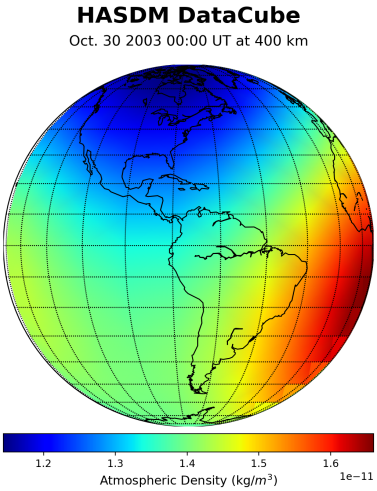

Fig. 1. HASDM database at 400 km on 2003/10/30 00:00 UT.

Figures 2a-t show the range of error for high and low solar activity. The one-sigma density error averages between 2–4% at high activity and 5–10% at low solar activity, depending upon altitude. There is higher uncertainty in HASDM at low solar activity for high altitudes because the atmosphere is thinner and there is a weaker signal in drag observations.

Machine Learning Characterization of the HASDM database

As part of this work, our team developed a machine learning (ML) capability to examine both the statistical uncertainty of the HASDM density database and the beginnings of an algorithm to replicate the database using a set of drivers. This algorithm is a prototype for a model called HASDM-ML. In this analysis, we:

- examined a Principal Component Analysis (PCA) method for identifying the dominant modes for both JB2008 and HASDM;
- trained a prototype ML model on HASDM and JB2008 data for comparison, referred to as HASDM-ML and JB08-ML, respectively; and
- investigated Monte Carlo (MC) dropout as a method for approximating model uncertainty.

To evaluate satellite drag coefficients, satellite drag for a number of reference satellites was computed over the span of ~10 years. These observed drag values were compared with modeled drag using a number of drag coefficient

models. The ratio of observed to modeled drag was then computed as a function of altitude to determine which drag coefficient model resulted in values that were closest to unity across the widest range of altitudes. A drag correction model is fit to the ratios and when applied to drag computation using META-HASDM, results in an unbiased drag estimate.

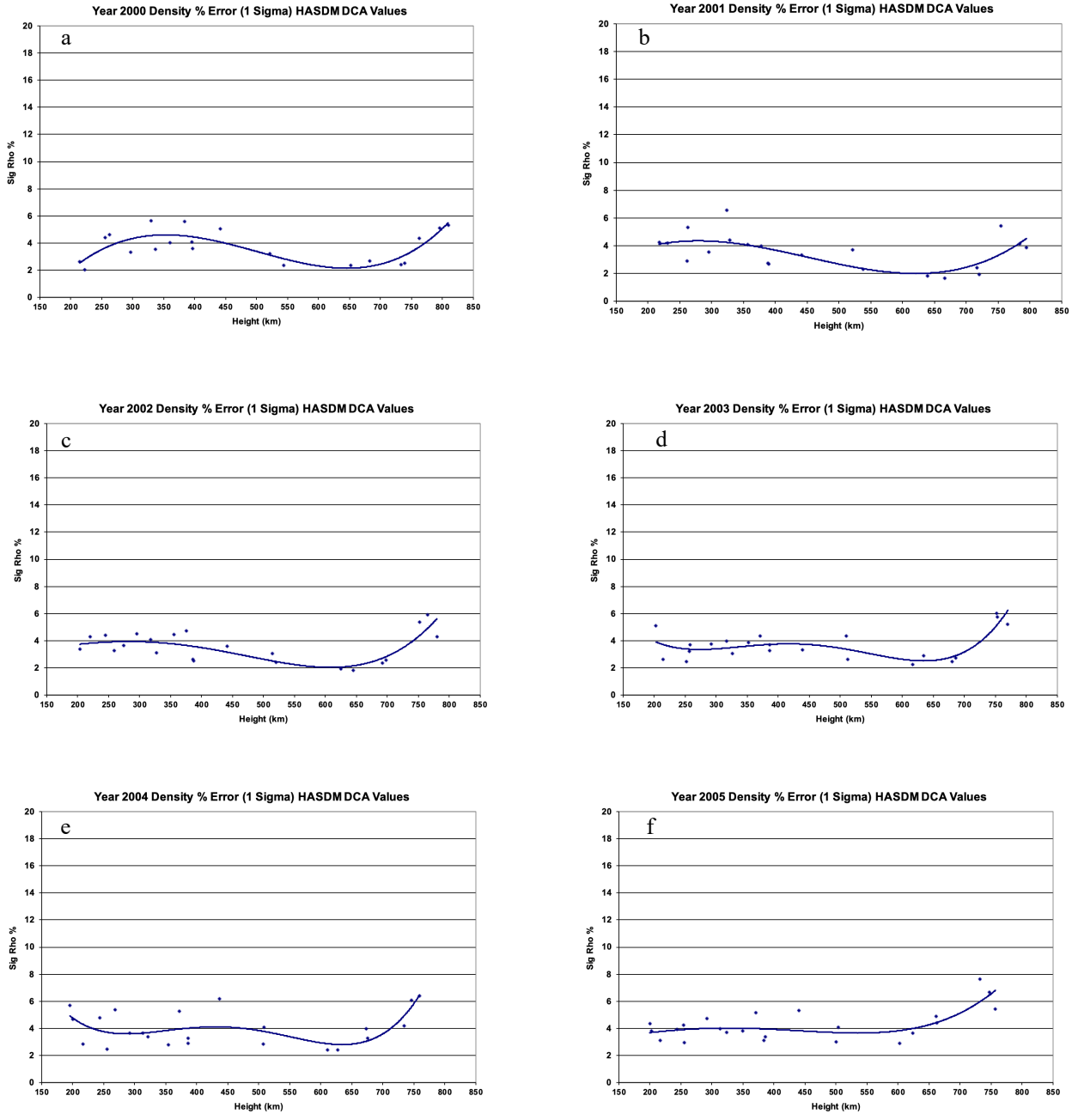

Fig. 2a-f. The range of error in the HASDM database from 2000-2005.

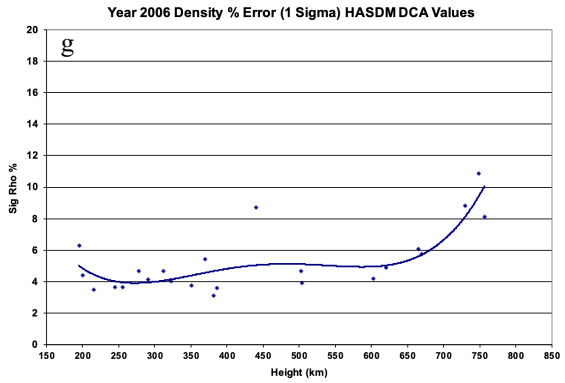

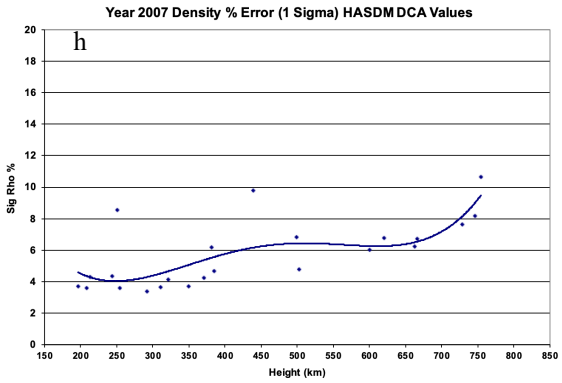

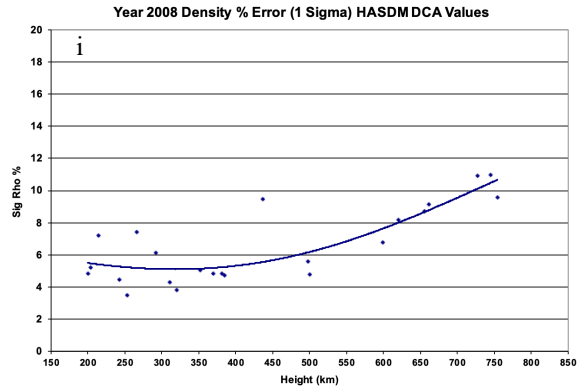

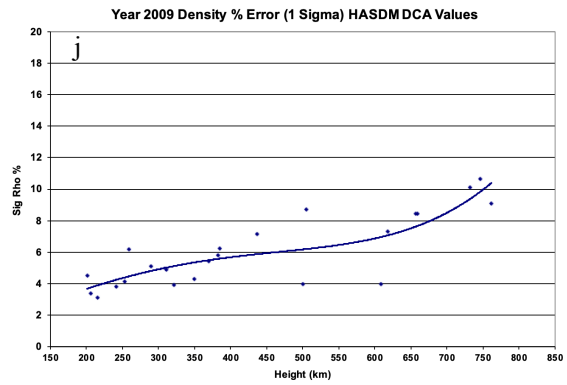

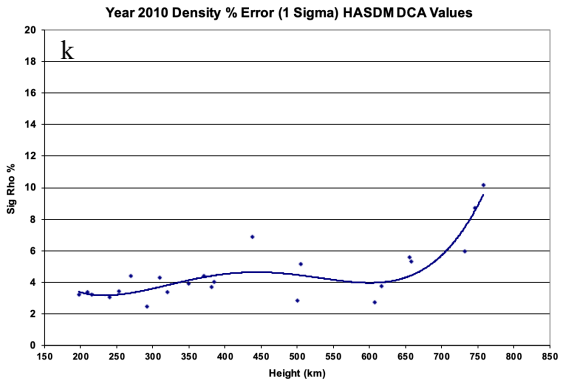

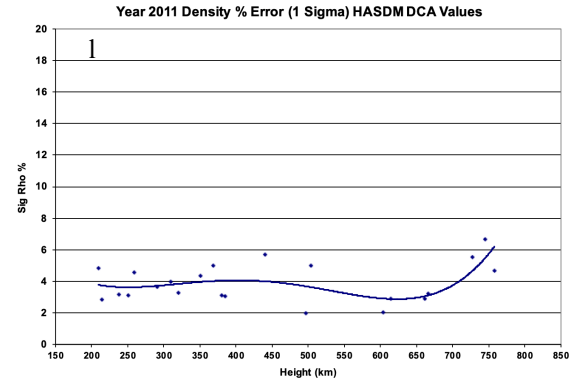

Fig. 2g-l. The range of error in the HASDM database from 2006-2011.

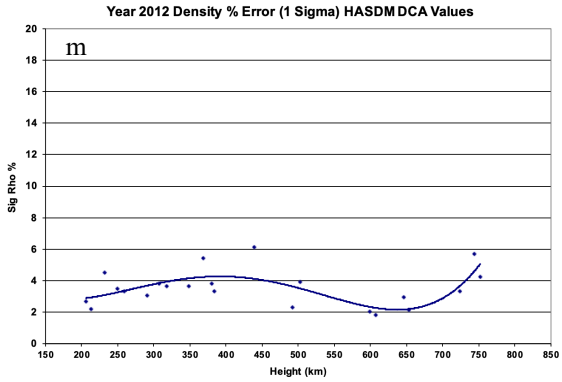

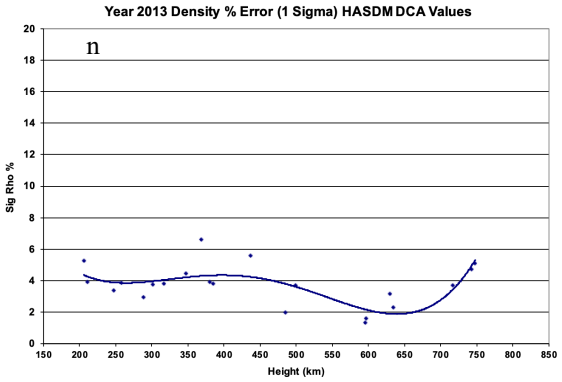

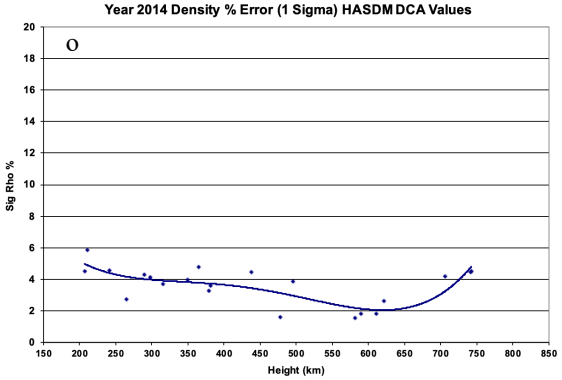

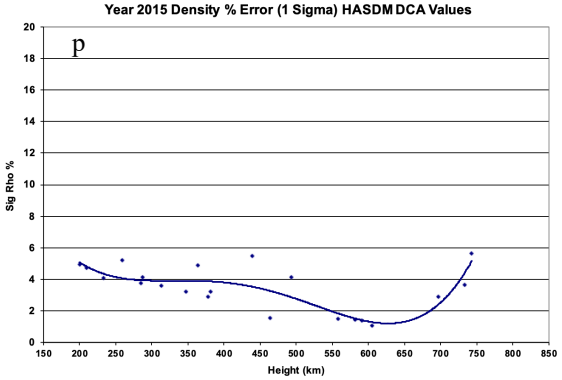

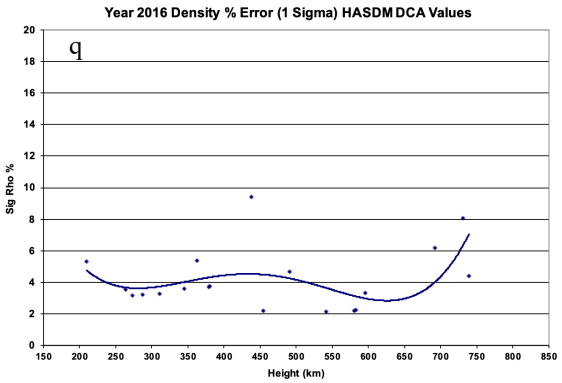

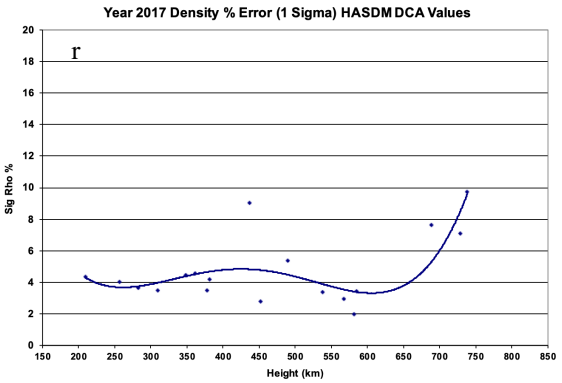

Fig. 2m-r. The range of error in the HASDM database from 2012-2017.

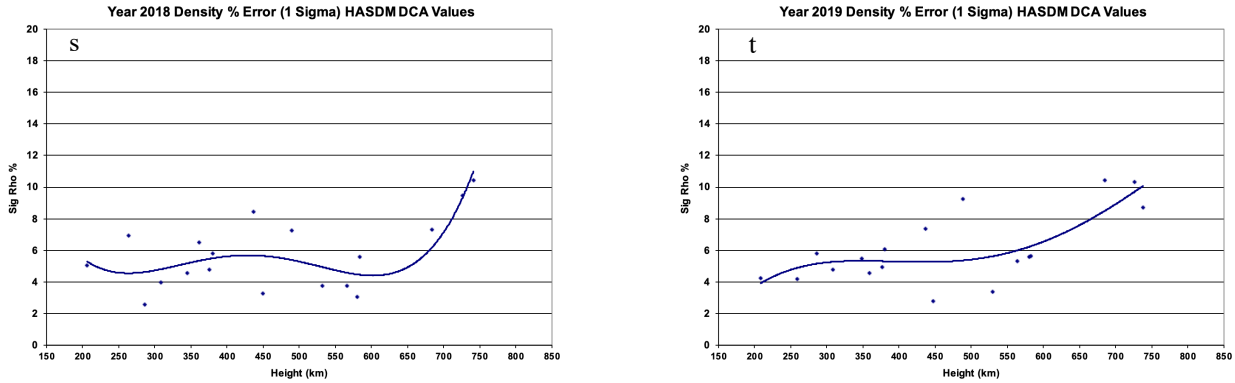

Fig. 2s-t. The range of error in the HASDM database from 2018-2019.

3. RESULTS

Dominant Modes of Variation.

Principle Component Analysis (see for example [5]) was performed on the 3D density grids between 2000 and 2019 (Fig. 3). The first three coefficients ($\alpha_1 - \alpha_3$) show parallels between the largest sources of variance in JB2008 and HASDM. The HASDM higher order coefficients ($\alpha_4 - \alpha_{10}$) show a much weaker signal. In Fig. 4, we show a summary of the energy (signal) captured in the first 20 PCA modes for the two density datasets. The term "energy" is the variance corresponding to eigenvalues, not physical energy. The first mode for JB2008 captures more energy than that of HASDM (left panel) and the cumulative energy (right panel) shows that the first ten modes capture 98% of JB2008 energy compared to only ~90% of the energy captured in the first ten modes in HASDM.

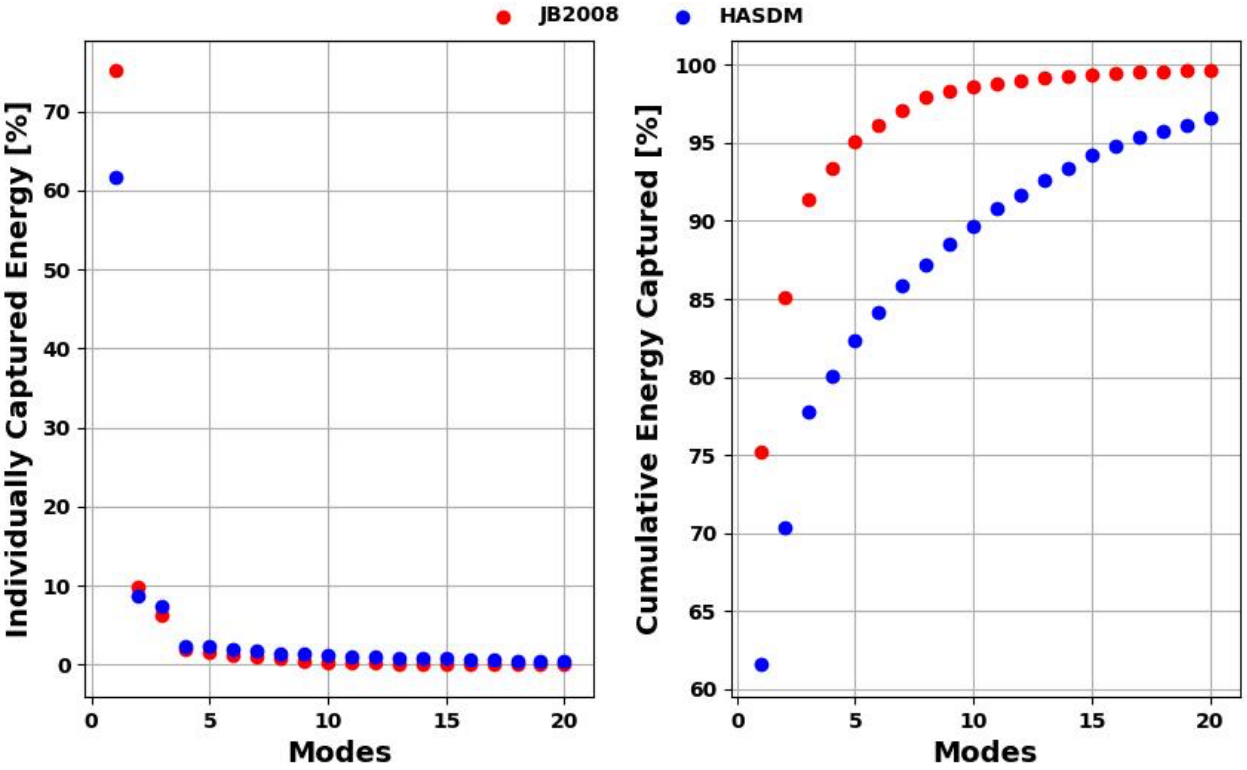

Fig. 3. The first ten coefficients of the HASDM dataset and JB2008 model density outputs for 2000–2019.

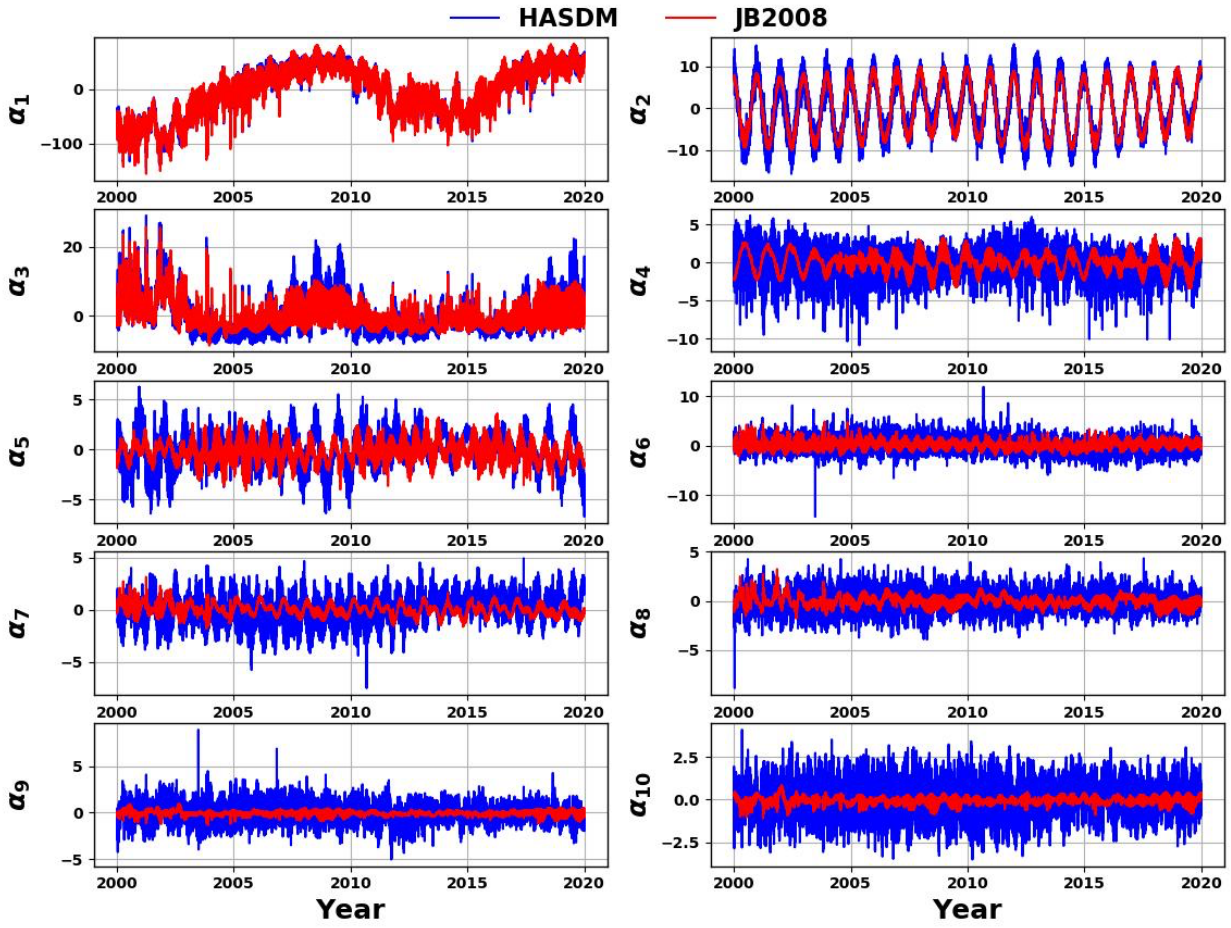

Fig. 4. Individual (left panel) and cumulative (right panel) energy captured by the first 20 PCA modes.

These results indicate that HASDM is a more complex system than JB2008; it captures additional dynamics that are not modeled by JB2008. This is because HASDM is a data assimilative system that has incorporated information content from dozens of calibration satellites at any given epoch compared to the deterministic core JB2008 (JBH09) model using only solar and geomagnetic drivers.

Model Performance

We used several architectures to understand how to model both HASDM and JB2008 densities and quantify their error. These architectures included: a) dense model using PCA coefficients or from other nonlinear dimensionality reduction techniques as outputs, e.g., Convolutional Autoencoders; b) dense model using reshaped density vectors as outputs; and c) combined dense-convolutional model using 3D density grids as outputs. In Fig. 5, we show results for feedforward neural networks as the Mean Absolute Error (MAE) for the two density databases.

We trained the HASDM-ML model and used the current optimal architecture to develop the JB08-ML. With identical architectures, hyperparameters, and inputs, JB08-ML is able to regress on its dataset much more effectively than HASDM-ML. The poorer performance with HASDM-ML is because of additional physical processes existing within the HASDM dataset that are not represented using the current set of inputs. We think these unmodeled physical processes may be related to inputs lacking for solar wind connectivity to the magnetosphere (including high-speed streams) that lead to increased Joule heating and particle precipitation. In addition, NO cooling on geomagnetic storm timescales, CO_2 thermospheric cooling that is pronounced during solar minimum periods, oxygen (O) and helium (He) abundance changes at high altitudes from solar minimum to maximum, as well as dynamics such as winds, waves, and tides are not modeled with input drivers.

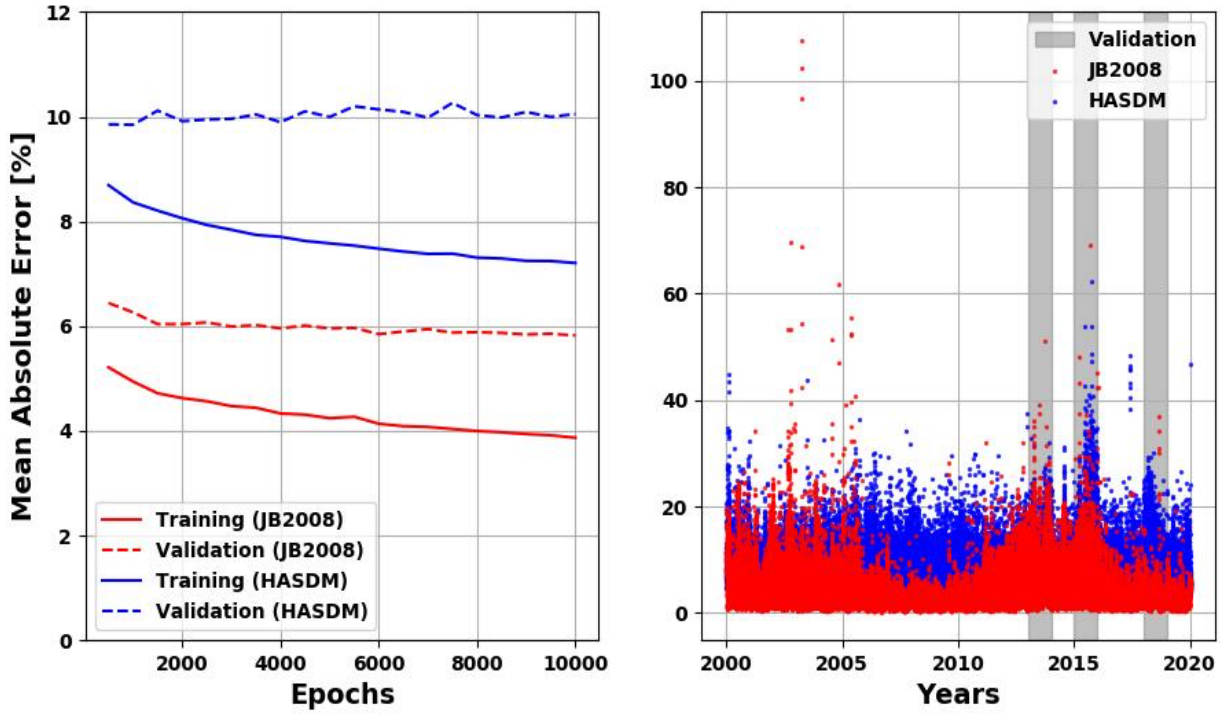

Fig. 5. Progression of mean absolute error with training (left panel) and for each time step (right panel)

It is this modeling deficit for HASDM-ML that we will correct during ongoing efforts. For example, when looking at MAE with respect to altitude, we noticed that there were distinct trends common between the models. Fig. 6 shows the altitude error profiles for both HASDM-ML and JBO8-ML during different solar activity levels. There is a pronounced peak in the lowest solar activity level (F10.7 $\leq$ 75 sfu) that resides around 500 km, and it rises in altitude with increasing solar activity. We hypothesize that this is likely the models' inability to capture the He/O transition effectively with the current set of inputs.

Another example is the uncertainty in HASDM during large solar storm conditions. Fig. 7 presents the density (kg m^{-3}) during the 7-day 2003 Halloween storm period at 400 km altitude and 3-h time granularity.

The HASDM database values, the mean value, and the 3σ bounds are shown. By manipulating dropout layers in the Monte Carlo method, the initially deterministic method is able to make probabilistic predictions for the density grids. MC dropout has been shown to function as a Bayesian approximator for method un-certainty and was applied to HASDM-ML. In theory, an infinitely wide layer with MC dropout estimates a Gaussian Process [6]. The 3σ bounds for the HASDM-ML prediction capture the SET HASDM database densities for nearly the entire 7-day period. A key observation is how the uncertainty grows with increased geomagnetic activity.

Error Characterization

The principal component analysis revealed the similarities between the first three modes, resulting in largest variance, but the higher order coefficients require further investigation and an inclusion of added drivers.

The performances of JB08-ML and HASDM-ML indicate a stronger correlation between the input set to the simpler JB2008 densities than that of the more complex HASDM densities. To remedy this, we will acquire added indices in Phase II for capturing more of the physical processes represented in the dataset. We will optimize the architecture and hyperparameters with tools such as AutoKeras [7].

We also investigated Gaussian process regression (GPR), which is an accurate and robust supervised machine learning technique, as a possible alternative ML method. The GPR method has been successfully applied to satellite drag coefficient [8] and neutral thermosphere mass density [5,9] modeling. In the process of evaluating GPR in the context of HASDM density analysis, we learned the following:

- the GPR method is not as well suited for training models with multiple outputs. For example, if we needed 10 PCA scores to represent the data cube, we would need to train 10 different GPR models. The GPR modeling cannot be used when the model output is the full 3D density grid as is the case with the HASDM data;
- the complexity of training a GPR model is $O(n^3)$, where n is the number of data points. Therefore, cost of training a GPR on two solar cycles worth of data is extremely high. We trained a model on 10 years of HASDM data. We also trained a neural net model on the same 10 years of data; and
- the neural network model outperformed the GPR in terms of error and model size. The total size of the saved model for GPR was over 6 GB while that for the neural network model was merely a few MB.

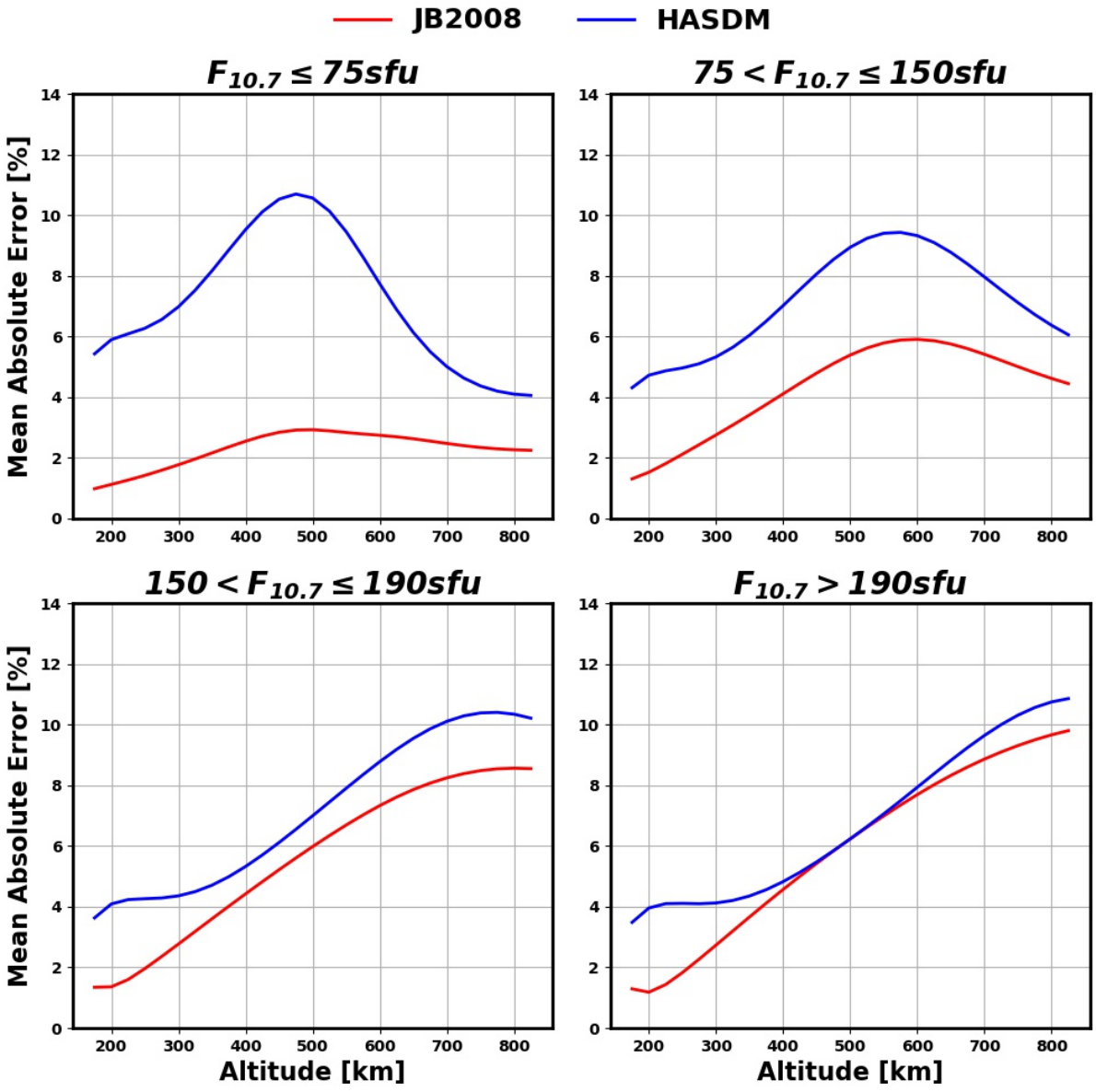

Fig. 6. Altitude error profiles for both HASDM-ML and JBO8-ML during different solar activity levels

Model-Consistent Drag Coefficient

One of the goals of this study is to evaluate ballistic coefficient that were consistent with META-HASDM below and above 500 km altitude. The ballistic coefficient is the product of satellite cross sectional area, its drag coefficient, divided by the mass ($C_D \times A/m$). Two types of drag coefficient models were evaluated, (a) the model used within

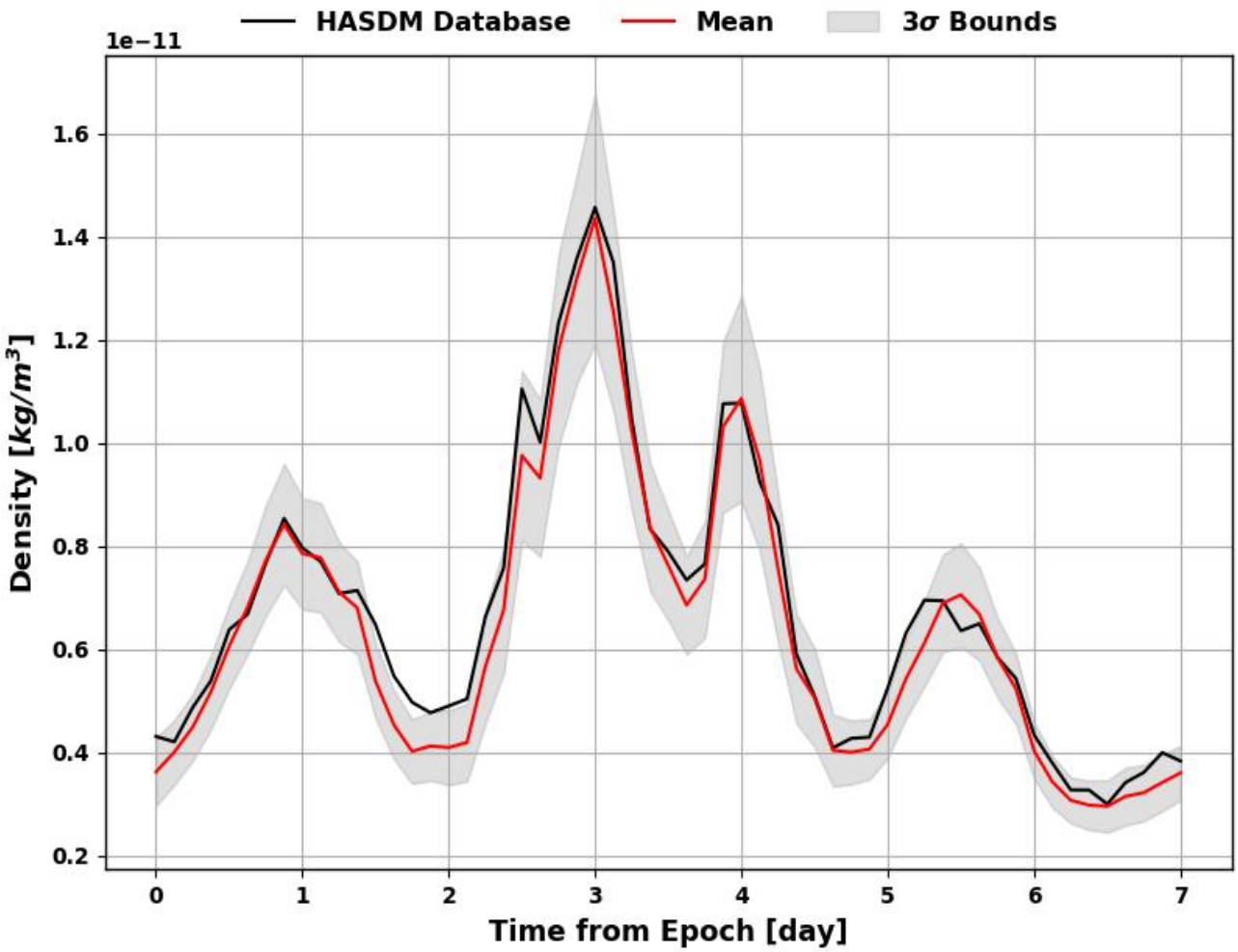

Fig. 7. HASDM density vs. time from epoch in days and with a 3-h time granularity

HASDM when assimilating satellite drag, (b) the Semi-Empirical Satellite Accommodation Model (SESAM) [10] applied to a Diffuse Reflection with Incomplete Accommodation (DRIA) C_D model [10].

The HASDM ballistic coefficients are based on fits of 30-y ballistic coefficients (B_{30yr}) and the range of documented A/m agrees with these values to ±10% (Bowman et al., 2004, i.e., AAS 04-173). The C_D used within HASDM is convolved with the B_{30yr} and is therefore consistent with any biases in the background atmospheric model. HASDM uses a fixed C_D value below 500 km and a C_D model presented by Afonso et al. [11] above 500 km. The C_D criteria by altitude are:

$$C_D = \begin{cases} 2.25, & h_p < 500\ km \\ C_{D,alt} & h_p \geq 500\ km \end{cases}$$

Depending on whether the orbit eccentricity is above or below a threshold value (e_{max}=0.01), the daily average C_D is then computed using the daily average value of the C_D along the orbit or the periapsis C_D value. These C_D criteria by eccentricity are:

$$C_{D,alt} = \begin{cases} \langle C_{D,Afns} \rangle_{orbit}, & e < e_{max} \\ C_{D,Afns}\big|_{hp}, & e \geq e_{max} \end{cases}$$

$$C_{D,Afns} = \begin{cases} \delta\left[\frac{8}{3}\left(\frac{V_T}{V_S}\right) + \frac{8}{15}\left(\frac{V_S}{V_T}\right)\right], & V_S < V_T \\ \delta\left[2 + \frac{4}{3}\left(\frac{V_T}{V_S}\right)^2 - \frac{2}{15}\left(\frac{V_T}{V_S}\right)^4\right], & V_S \geq V_T \end{cases}$$

$$V_T = \left(\frac{8kT}{\pi m}\right)^{1/2}$$

The parameters of the Afonso drag coefficient model, CD,Afns, are described fully in reference [11]. The model is dependent of the thermal velocity, V_T, relative to the satellite velocity, V_S.

SESAM+DRIA bases the energy accommodation on the pressure of atomic oxygen and applies this to a diffuse reflection model [10].

Calibrated A/m values (Table 1) can be used to evaluate C_D model compatibility with HASDM along a range of effective densities / altitudes. These values are applied to energy dissipation rates calculated using mean mean-motion changes in an 8-day moving analysis of two-line element data. Details of energy dissipation rate (EDR) calculations can be found in work by Picone et al., Bernstein et al., and Pilinski et al. [12,13,10]. We then compare energy dissipation rate ratios (observed vs. modeled) using the HASDM and SESAM+DRIA C_D models by averaging all data between 2000 and 2011. The resulting averages of the observed to modeled EDR ratios are illustrated in Fig. 8. The error bars represent the variability of the annual average ratios. Correction functions that make the drag computed using each C_D model "compatible" with HASDM are shown below their respective panels. The HASDM C_D model (left panel of Fig. 8) results in the best long-term stability but exhibits an altitude-dependent bias below 500 km (where this C_D model uses a fixed value). A likely explanation for this bias is that the A/m values used internally by HASDM when performing drag assimilation are offset from the calibrated values in Table 1 in a way that compensates for this low-altitude offset. The SESAM+DRIA model (right side of Fig. 8) has relatively low amounts of altitude variability but results in higher inter-annual variability for the estimated drag computation.

Table 1: Calibrated A/m values

NORAD ID	Name	Perigee Alt. [km]	Apogee Alt. [km]	i	Apriori A/m	HASD Calibrated A/m	MSIS Calibrated A/m	Combined Calibration	30-yr A/m
6073	Venus Lander (COSMOS 482)	200	2172	52	0.00140 (±93%)	0.00179 (±1%)	0.00188 (±5%)	0.00181 (±2%)	0.0016
22	Explorer VII	506	678	50	0.01065 (±2%)	-	-	-	-
7337	KOSMOS 660 (Taifun Cal Sphere)	373	1146	83	0.00541 (±11%)	0.00534 (1±%)	0.00532 (±2%)	0.00534 (2%)	0.0050
8744	KOSMOS 807	372	1184	83	0.00541 (±11%)	0.00531 (±2%)	0.00528 (±1%)	0.00530 (2%)	0.0050
12138	KOSMOS 1238	390	1426	83	0.00541 (±11%)	0.00535 (±1%)	0.00524 (±1%)	0.00531 (2%)	0.0050
14483	KOSMOS 1508	385	1476	83	0.00541 (±11%)	0.00537 (±1%)	0.00536 (±3%)	0.00537 (2%)	0.0050
20774	KOSMOS 2098	387	1587	83	0.00541 (±11%)	0.00545 (±1%)	0.00546 (±2%)	0.00546 (2%)	0.0050
23278	KOSMOS 2292	395	1700	83	0.00541 (±11%)	0.00538 (±1%)	0.00522 (±1%)	0.00531 (2%)	0.0050
12388	KOSMOS 1263	395	1338	83	0.00541 (±11%)	0.00532 (±1%)	0.00530 (±1%)	0.00531 (1%)	0.0050
2909	SurCAL NRL 150B / Calsphere 4	749	755	70	0.0834 (±2%)	-	-	-	-
2826	SurCAL NRL 160 / Calsphere 3	775	787	70	0.0815 (±1%)	-	-	-	-
11	Vanguard 2	556	2937	33	0.0213 (±7%)	0.02237 (±4%)	0.02148 (±5%)	0.02196 (5%)	0.0224
4382	DFH-1	428	2034	68	0.0045 (±10%)	0.00511 (±1%)	0.00493 (±3%)	0.00504 (3%)	0.0050
Interim Reference Satellites:									
26929	Starshine III			67	0.00776 (±1%)	-	-	-	-
29664	ANDE RR, MAA			52	0.00352 (±2%)	-	-	-	-
29667	ANDE RR, Fcal			52	0.00251 (±2%)	-	-	-	-
35694	ANDE 2, Castor			52	0.00386 (±2%)	-	-	-	-

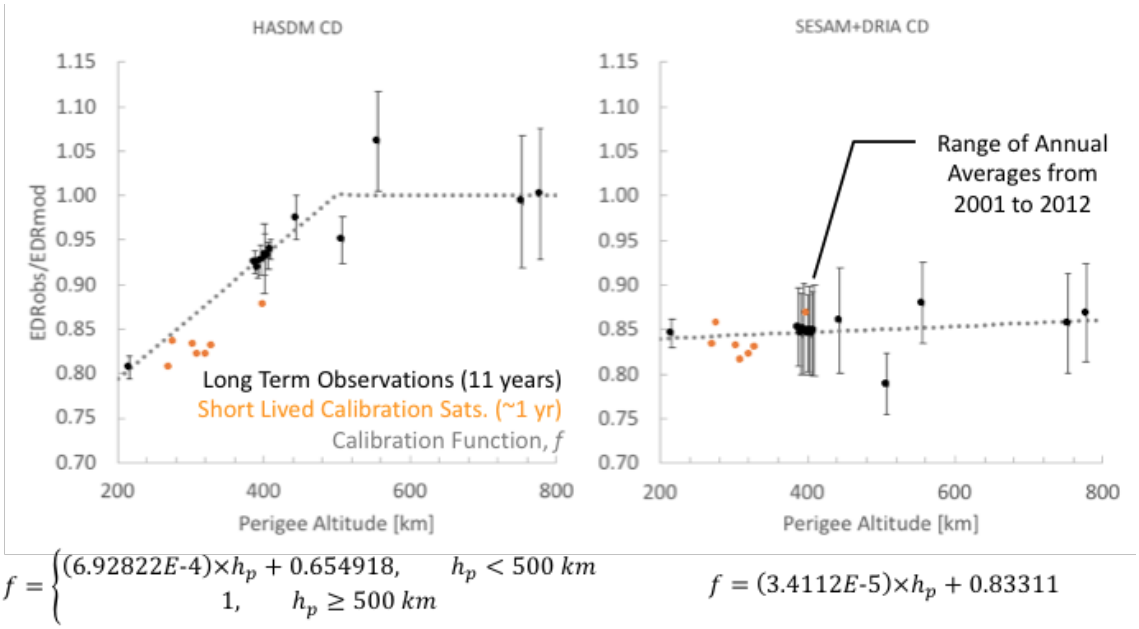

Fig. 8. CD fits for HASDM and SESAM+DRIA with the associated calibration functions, f, indicating corrections needed.

We can validate these results using satellites not used in the calibration and launched after the calibration period. We used the DANDE and POPACS spheres [14] along with four other satellites listed at the bottom of Table 1 and compared their observed drag with the values resulting from HASDM and the calibrated C_D between 2014 and 2017. The orange symbols in Fig. 8 represent these shorter-lived calibration spheres (interim reference satellites in Table 1). Note that these objects have well documented as-flown A/m ratios with low uncertainty but were not used in the derivation of the correction functions. We see that these generally agree with the model correction functions within 2%-5%. Based on this result, when computing drag using the HASDM database or the META-HASDM model, we recommend the use of the HASDM C_D model with the altitude-dependent drag correction function shown in Figure 8. Figure 9 demonstrates the use of the correction function by comparing the EDR computed using HASDM and the corrected C_D model with TLE-derived EDR's for the DANDE spherical satellite [14].

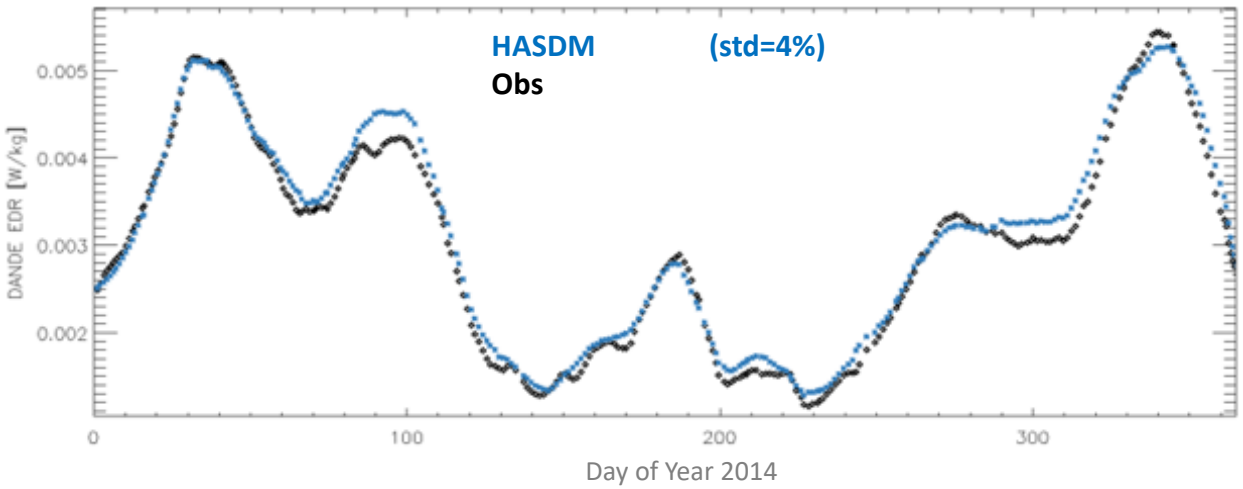

Fig. 9. Calibration of DANDE satellite in 2014 with HASDM EDRs (blue) and the TLE-derived EDRs (black).

4. CONCLUSIONS

In this paper we demonstrated the feasibility of an empirical model based on 20 years of HASDM outputs, taking advantage of nearly two solar cycles of satellite drag observations from ~70 calibration satellites. The resulting model, META-HASDM, does not yet outperform leading empirical models such as Jacchia-Bowman 2008. However, we have identified several methods for enhancing META-HASDM including additional parameters such as location relative to the Oxygen-Helium transition. In addition to this, we have published the HASDM-compatible drag coefficient model along with an altitude dependent correction function. Using this model along with the publicly released HASDM database or with the new META-HASDM density model presented here, results in drag predictions that are unbiased on average with respect to observations.

5. REFERENCES

[1] Storz, M. F., B. R. Bowman, M. J. I. Branson, S. J., Casali, and W. K. Tobiska (2005). High accuracy satellite drag model (HASDM). *Advances in Space Research*, *36*(12), 2497-2505.

[2] Hejduk, M. D. and D. E. Snow (2018). The effect of neutral density estimation errors on satellite conjunction serious event rates. Space Weather, 16, 849–869. https://doi.org/10.1029/2017SW001720.

[3] Tobiska, W.K., B.R. Bowman, D. Bouwer, A. Cruz, K. Wahl, M. Pilinski, P.M. Mehta, and R.J. Licata (2021), The SET HASDM database, Space Weather Journal, in press. https://doi.org/10.1002/essoar.10504902.1

[4] Space Weather Operations, Research, and Mitigation Working Group; Space Weather, Security, and Hazards Subcommittee; Committee on Homeland and National Security of the National Science and Technology Council, The White House, *National Space Weather Strategy and Action Plan*, March 2019.

[5] Mehta, P. M. and R. Linares (2017), A methodology for reduced order modeling and calibration of the upper atmosphere, Space Weather, 5, doi:10.1002/2017SW001642.

[6] Gal, Y. and Z. Ghahramani (2016), Dropout as a Bayesian approximation: Representing model uncertainty in deep learning, in *International conference on machine learning, IEEE Trans. Knowl. Data Eng.*, vol. 28, no. 4.

[7] Jin, H., Q., Song, and X. Hu (2019), Auto-Keras: An Efficient Neural Network Search System, in *Proceedings of the 25th ACM SIGKDD International Conference*, http://arxiv.org/abs/1806.10282.

[8] Mehta, P. M. A. Walker, E. Lawrence, R. Linares, D. Higdon and J. Koller (2014), Modeling Satellite Drag Coefficients with Response Surfaces, Advances in Space Research, Vol. 54, No. 8, 2014, pp.1590-1607.

[9] Mehta, P. M., R. Linares, and E. K. Sutton (2019), Data-driven inference of thermosphere composition during solar minimum conditions, *Space Weather*, 17, 1364–1379, https://doi.org/10.1029/2019SW002264.

[10] Pilinski, M. D., B. M. Argrow, S. E. Palo (2013), A Semi-Empirical Satellite Accommodation Model for Spherical and Randomly Tumbling Objects, Journal of Spacecraft and Rockets, doi: 10.2514/1.A32348.

[11] Afonso G., Barlier F., Berger C., Mignard F., Walch J. J. (1985), Reassessment of the Charge and Neutral Drag of Lageos and its Geophysical Implications, Journal of Geophysical Research, Vol 90, No 811, pp. 9381-9398, September 30, 1985

[12] Picone, J., Emmert, J., and Lean, J. (2005), Thermospheric densities derived from spacecraft orbits: Accurate processing of two-line element sets, Journal of Geophysical Research: Space Physics, Vol. 110, No. A3, 2005.

[13] Bernstein, V., Pilinski M. D., Sutton, E. K., (2021) Assessing Thermospheric Densities Derived from Orbital Drag Data, Proceedings of the 31st AAS/AIAA Space Flight Mechanics Meeting, AAS 21-354, 2021

[14] Pilinski M.D., McNally, L., Bowman, B., Palo, S., Forbes, J., Davis, B., Moore, G. R., Kemble, K., Koehler, C., Sanders, B., (2016) Comparative Analysis of Satellite Aerodynamics and Its Application to Space-Object Identification, Journal of Spacecraft and Rockets, Vol. 53, No. 5, Sep-Oct 2016, https://doi.org/10.2514/1.A33482